Remote Sensing Inversion of the Total Suspended Matter Concentration in the Nanyi Lake Based on Sentinel-3 OLCI Imagery

Yong Xie, *Senior Member, IEEE*, Yanting Zhou, Zui Tao, Wen Shao, and Meng Yang

***Abstract*—Herein, in situ water reflectance and TSM data obtained from several experiments on the Nanyi Lake from 2018 to 2022 and the Sentinel-3 Ocean and Land Colour Instrument (OLCI) satellite synchronization data were used to compare four atmospheric correction methods (FLAASH, 6S, ACOLITE, and C2RCC) and construct an empirical model for TSM inversion in the Nanyi Lake to analyze the spatial and temporal changes in the water quality in the Nanyi Lake from 2018 to 2023. On the Sentinel-3 OLCI data, the C2RCC algorithm showed the highest accuracy and overall performance stability (RMSE: 0.0014–0.0051 Sr^{-1}, MAPE: 18.44%–68.47%, and BIAS: from −3.68% to 23.63%). The highest correlation was observed between the three-band ratio (B9 + B18)/B10 and the in situ TSM; the TSM inversion model constructed based on this inversion factor showed the best accuracy for the Nanyi Lake (R^2: 0.76, RMSE: 5.01 mg/L, and MAPE: 28.46%). The spatial and temporal changes in TSM in the Nanyi Lake exhibited significant regularity. Specifically, the TSM was higher in 2018–2019, significantly decreased in 2020, and stabilized in 2021–2023. Owing to the effects of human activities, precipitation, and illumination, seasonal variation in the TSM in the Nanyi Lake was detected, with TSM decreasing in the following order: summer > autumn > spring > winter. Concerning spatial variations, high TSM was observed in the northwest, northeast, and southeast of the Nanyi Lake reclamation area and its surrounding lake area. River confluence and human activities affected the area, leading to significant fluctuations in TSM in 2018–2023.**

***Index Terms*—Atmospheric correction, Nanyi lake, remote sensing retrieval, total suspended matter (TSM).**

I. Introduction

TOTAL suspended matter (TSM) refers to the concentration of solids suspended in water, including insoluble inorganic and organic matter in water, as well as mud, sand, clay, microorganisms, etc., [1]. TSM not only affects water transparency, underwater light field, and primary productivity [2], but also directly impacts the balance of aquatic ecosystems [3]. Therefore, monitoring the concentration and distribution of TSM is of great significance for preventing and controlling water pollution in inland water bodies. The traditional method of TSM monitoring is field sampling followed by drying and weighing in the laboratory. The primary drawback of this method is that it is time-consuming and labor-intensive, making it impractical for conducting long-term, large-scale monitoring [4], [5]. Remote sensing, which is characterized by large spatial coverage, short monitoring cycles, long dynamic time series, and low cost [6], [7], can reveal the migration of pollutants and pollution sources, which is challenging to detect using conventional methods [8]. Therefore, an increasing number of experts and scholars are using remote sensing for the quantitative inversion of TSM to monitor water environments.

Currently, algorithms for estimating TSM using remote sensing can be broadly classified into two categories: semianalytical and empirical. However, there is still no unified model for different types of lakes [9]. Semianalytical models are based on the inherent optical properties of water and use remotely sensed reflectance to invert the color components of water. The common semianalytical algorithms include APPLE [10] and three-band model [11]. Huajie et al. [12] selected 710 nm as the reference wavelength for the semianalytical algorithm by determining the nonwater absorption coefficient at 400–800 nm, calculating the backscattering coefficient at various wavelengths, and linearly fitting them with the TSM, achieving an R^2 of 0.915. Although the semianalytical models have certain physical significance, their construction requires measuring multiple optical parameters of water, making the models relatively complex. Empirical models are constructed on the basis of simultaneously measured water TSM and remote sensing spectral data, establishing a quantitative relationship between TSM and the optical properties of water. Wirabumi et al. [13] employed four conventional spectral bands of PlanetScope imagery for empirical modeling of TSM at different effective water depths, with results indicating that band ratios are optimal inversion factors. Jensen et al. [14] compared empirical algorithms for estimating TSM using both hyperspectral and multispectral data based on measured water spectra and their first derivatives. They selected the optimal empirical model and applied it to different remote sensing data sources and regions to assess the robustness and transferability of the algorithm. With the development of computer science and artificial intelligence in recent years, machine learning has been widely used for TSM modeling [15], [16]. Specifically, Silveira et al. [17], employed various machine learning methods, based

Manuscript received 13 March 2024; revised 13 May 2024; accepted 16 May 2024. Date of publication 20 May 2024; date of current version 30 May 2024. This work was supported in part by the National Natural Science Foundation of China under Grant 42176176 and in part by the Land Observation Satellite Supporting Platform of the National Civil Space Infrastructure Project. *(Corresponding author: Zui Tao.)*

The authors are with the School of Geographical Sciences, Nanjing University of Information Science and Technoloy, Nanjing 210044, China (e-mail: xieyong@nuist.edu.cn; zyt981127@163.com; taozui@aircas.ac.cn; wenshao@nuist.edu.cn; meng_yang9902@163.com).

Digital Object Identifier 10.1109/JSTARS.2024.3402963

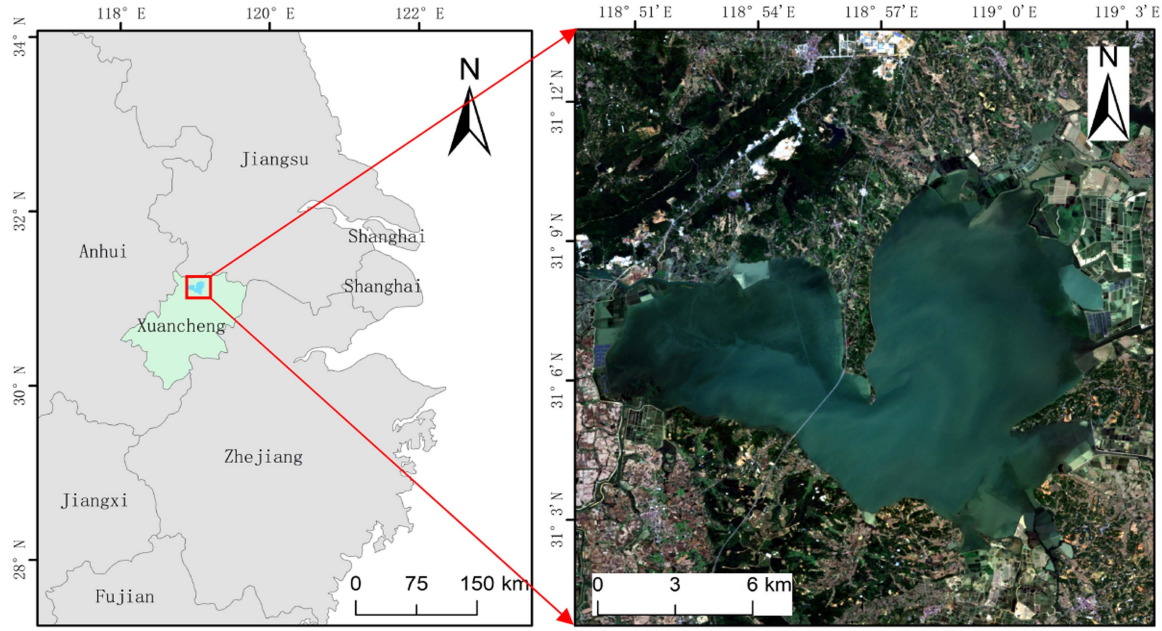

Fig. 1. Location and satellite image of the study area.

on Sentinel-3, for TSM inversion in the Missouri and Mississippi rivers, achieving R^2 greater than 0.8. Common machine learning techniques such as neural networks [18], CatBoost [19], and Random Forest [4] have also been extensively used in TSM inversion. Although machine learning offers certain advantages in TSM inversion, it requires a large amount of training data to avoid overfitting. Therefore, the empirical method remains a simple and accurate approach for suspended sediment concentration inversion in regional water bodies [20].

The Nanyi Lake is the largest lake in southern Anhui and serves as a vital water source for the local people [21]. Affected by human activities such as enclosuring and farming along the lake, the area of the Nanyi Lake has decreased by approximately 57.37 km^2 [22] between 1985 and 2016. Owing to the impact of sediment input from the watershed, the lakebed has experienced severe siltation [23]. Wind and waves induce sediment suspension, leading to decreased water transparency and deterioration of water quality. Since 2017, fluctuations in water quality have been observed in the Nanyi Lake. According to publicly available data from the People's Government of Xuanzhou District, Xuancheng City, the overall water quality transitioned from Class IV in 2018 to Class III in 2021, and the lake became mesotrophic. In 2022, the water quality in the central areas of West Lake and East Lake was Class III and Class IV, respectively. These variations highlight the fragile ecological water environment of the Nanyi Lake and warrant attention.

The accuracy of atmospheric calibration is a crucial factor influencing the precision of water quality parameter retrieval from satellite remote sensing data [24]. Herein, imagery from the next-generation water color sensor Sentinel-3 Ocean and Land Colour Instrument (OLCI) satellite was used to more accurately estimate the TSM in the Nanyi Lake and analyze the monthly change in TSM. In situ water spectra and TSM data for the Nanyi Lake were employed to evaluate atmospheric correction methods and empirical algorithms for TSM inversion. We used optimized algorithms to calculate the suspended sediment concentration in the Nanyi Lake from 2018 to 2023. This article further analyzed the spatiotemporal variation characteristics and distribution patterns of TSM, aiming to provide a scientific basis for water environment monitoring and management in the Nanyi Lake.

II. Data and Methods

A. Overview of the Study Area

The Nanyi Lake is located in Xuancheng City, Anhui Province (see Fig. 1). Its coordinates are approximately 118°50′3″–119°3′39″E and 31°1′17″–31°10′24″N. The total area of the lake is about 150 km^2. It has a subtropical humid monsoon climate with an annual average precipitation of 1168 mm. The water quality in the Nanyi Lake is generally categorized as Class III throughout the year, indicating a mild eutrophic state. However, in recent years, because of increased pollution loads from point and nonpoint sources within the watershed, the risk of eutrophication has sharply increased [25].

B. In Situ Measured Water Reflectance Data

The in situ data for this article were collected using the Nanjing Remote Sensing Authenticity Validation Site. To obtain more accurate and comprehensive hyperspectral and TSM data, the measured points were selected according to adaptive sample points fusion in weighted space [26] and navigational water experiments were used.

The water spectral data used in this article were obtained through in situ measurements using a dedicated instrument.

TABLE I
TIME AND NUMBER OF SAMPLING POINTS FOR THE MEASURED SPECTRA OF THE NANYI LAKE

Sampling Time	Number of Points	Sampling Time	Number of Points
2020.08.18	14	2021.10.29	11
2020.09.04	13	2021.11.19	11
2020.10.23	14	2022.06.15	14
2020.11.10	11	2022.07.01	12
2020.11.12	12	2022.08.01	12
2021.04.09	12	2022.08.02	12
2021.09.22	11	2022.09.19	13
2021.10.05	13	2022.10.18	14

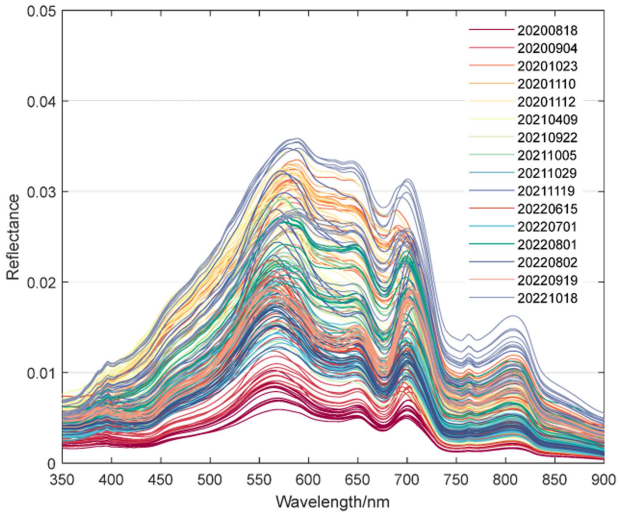

Fig. 2. Measured spectra of the Nanyi Lake.

Under clear, cloudless, and stable atmospheric conditions, the remote sensing reflectance of the water body was measured using a radiometric measurement system (TriOS, Germany), covering a spectral range of 320–900 nm. The water surface was measured using the above-water method [27], avoiding solar flares and ship shadows. Each sampling point was measured 15 times to ensure measurement accuracy. During 2020–2022, 16 sets of experimental data synchronized with the transit of Sentinel-3 satellites (±1.5 h) were selected to obtain the measured data at multiple time points. The specific sampling times and the number of sampling points are given in Table I.

The measured reflectance of water (see Fig. 2) shows differences in the reflectance values on different dates. The numerical differences between different sampling points on the same date are relatively small, which is related to the seasonal variation in water turbidity [28].

C. In situ TSM Measurement

Samples (300–500 mL) of surface water (depth: 30–50 cm) were collected at the actual measurement points and transported to the laboratory on the same day (stored in brown bottles at 4 °C). Following the national standard GB11901-89, the drying–weighing method was employed to determine TSM in the samples. Because of the homogeneity of water in the Nanyi Lake and the distance between the measured points being greater than 2 km, the coefficient of variation (CV) was used to assess the effective homogeneity of spectral values within a 3 × 3 window centered on each sampling point based on geographical coordinates and the spatial resolution (300 m) of the Sentinel 3 OLCI imagery. CV was calculated as the ratio of the standard deviation of DN (Digital Number) values to the mean, and data points with a CV greater than 15% [29] were excluded.

D. Remote Sensing Data

The Sentinel-3 satellite series consists of two satellites, 3A and 3B, equipped with the OLCI, which takes global multi-spectral medium-resolution images of the ocean and land. OLCI imagery obtained in the combined observation mode of 3A and 3B allows high-frequency observation with a revisit period of less than 2 days, enabling the monitoring of monthly TSM in the Nanyi Lake. In addition to the 15 bands of the MERIS sensor, the Sentinel-3 satellite features 6 additional bands, totaling 21 bands (see Table II), significantly enhancing the remote sensing capabilities for ecological indicators of marine and inland water bodies. Herein, we used Sentinel-3 L1C level data for 2018–2023, closely synchronized with the measurement time (±1.5 h). The images can be freely downloaded from the European Space Agency's official website (https://scihub.copernicus.eu/dhus/#/home).

III. EVALUATION OF THE ADAPTABILITY OF THE ATMOSPHERIC CORRECTION AND TSM INVERSION ALGORITHMS

A. Adaptability of the Atmospheric Correction Methods

Atmospheric correction of satellite imagery of water aims to extract the reflectance of water with information characterizing the water body from the total signal received by the sensor [30]. Currently, there is no universally applicable atmospheric correction method for different inland lake water bodies. Therefore, the exploration of atmospheric correction methods applicable to the Nanyi Lake and similar lakes using Sentinel-3 OLCI satellite data can improve the inversion accuracy. Herein, four commonly used atmospheric correction methods were employed: FLAASH [31], 6S [32], ACOLITE [33], [34] (suitable for inland turbid water bodies), and C2RCC [35], [36] (algorithm provided by the Sentinel's official platform). By combining in situ spectra with the spectral response functions of the Sentinel-3 OLCI satellite bands, the applicability of atmospheric correction methods was assessed to identify methods suitable for the Nanyi Lake and similar inland lakes.

Because the C2RCC algorithm uses the image information from bands 13–15 and 19–20 for atmospheric correction, the output results only include the visible (bands 1–12) and near-infrared bands (bands 16–18 and 21). Herein, only data from bands 1–12 and 16–18 were analyzed. The corrected reflectance for each band and the in situ reflectance were used to generate density plots (see Fig. 3) for an intuitive comparison of the overall data distributions. Errors for each algorithm in each band were calculated to analyze the accuracy of the algorithms for each band, as given in Table II.

TABLE II
SENTINEL-3 OLCI IMAGE BAND INFORMATION

Band	Center (nm)	Width (nm)	Band	Center (nm)	Width (nm)
Band 1	400	15	Band 12	753.75	7.5
Band 2	412.5	10	Band 13	761.25	2.5
Band 3	442.5	10	Band 14	764.375	3.75
Band 4	490	10	Band 15	767.5	2.5
Band 5	510	10	Band 16	778.85	15
Band 6	560	10	Band 17	865	20
Band 7	620	10	Band 18	885	10
Band 8	665	10	Band 19	900	10
Band 9	673.25	7.5	Band 20	940	20
Band 10	681.25	7.5	Band 21	1020	40
Band 11	708.75	10			

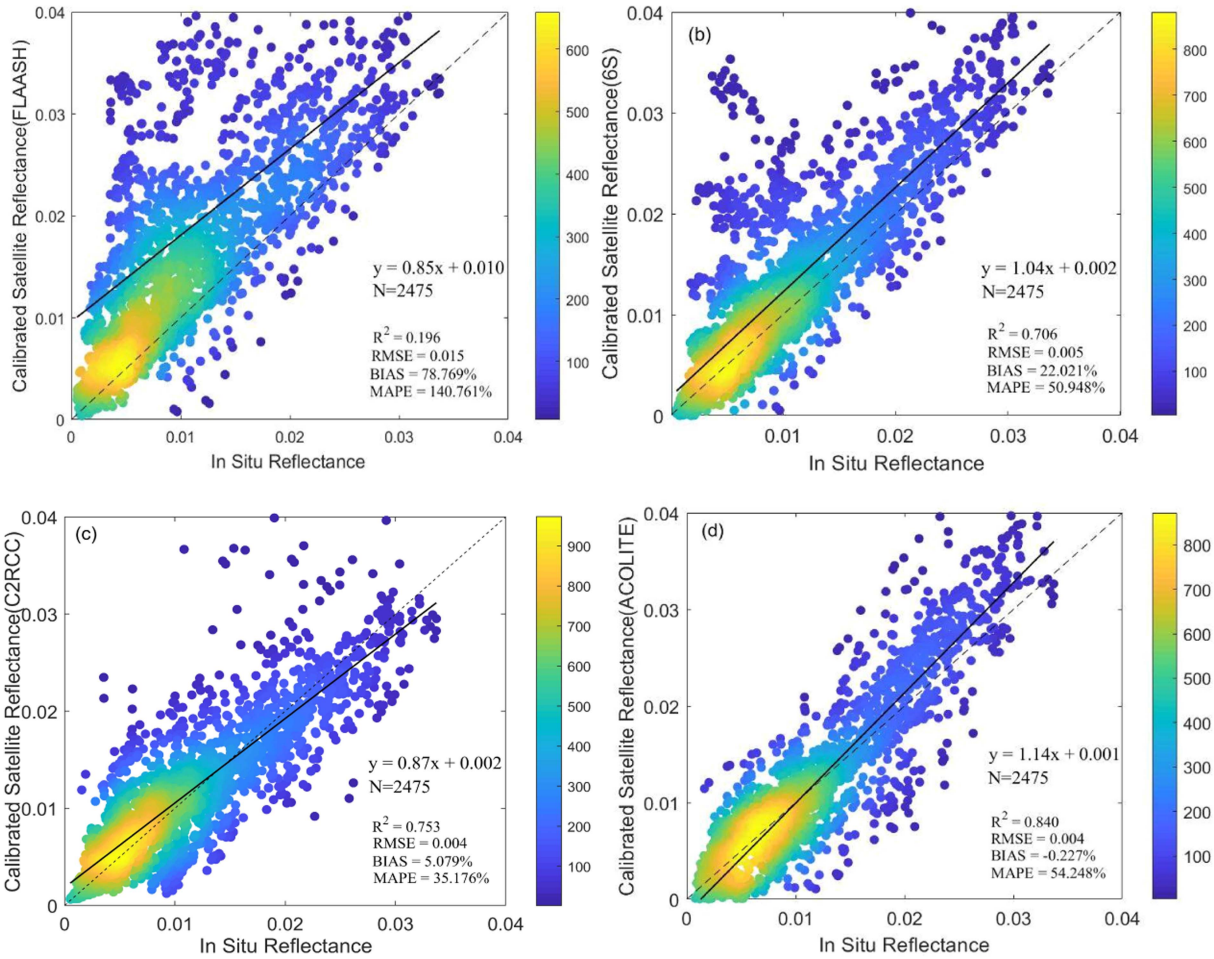

Fig. 3. Plot of measured reflectance versus corrected satellite reflectance density for different atmospheric correction algorithms: (a) FLAASH; (b) 6S; (c) C2RCC; and (d) ACOLITE.

As shown in Fig. 3, 6S and FLAASH overall overestimate atmospheric correction. FLAASH shows a bias of 78%, which was mainly attributed to the choice of atmospheric model and aerosol type. The C2RCC algorithm shows relatively stable correction performance across all bands, with a MAPE of 35.176%, which is the lowest error among the four algorithms. The ACOLITE algorithm exhibits the best fitting results, with R^2 reaching 0.840.

Based on the error magnitudes for each band (see Table III), the ACOLITE algorithm, which employs 6SV to generate a lookup table for Rayleigh scattering correction, is more optimal than other algorithms in shortwave bands (bands 1–5). ACOLITE was initially designed to correct imagery of high spatial resolution, even meter-resolution satellite imagery. Thus, as Sentinel-3 OLCI imagery has a resolution of 300 m, the

TABLE III
ATMOSPHERIC CORRECTION ACCURACY BY BAND

Wave band	FLAASH			6S			C2RCC			ACOLITE		
	RMSE (Sr^{-1})	MAPE (%)	BIAS (%)	RMSE (Sr^{-1})	MAPE (%)	BIAS (%)	RMSE (Sr^{-1})	MAPE (%)	BIAS (%)	RMSE (Sr^{-1})	MAPE (%)	BIAS (%)
Band 1	0.0373	601.45	488.66	0.0145	256.13	204.40	0.0044	62.04	0.41	**0.0032**	**46.68**	**25.83**
Band2	0.0268	398.64	308.27	0.0062	95.28	57.97	0.0046	68.47	7.65	**0.0026**	**38.37**	**8.57**
Band3	0.0249	338.33	247.67	0.0067	93.26	63.40	0.0051	65.83	8.32	**0.0027**	**33.86**	**9.49**
Band4	0.0145	118.55	88.29	0.0046	35.62	23.14	0.0047	39.27	6.03	**0.0029**	**21.26**	**−3.87**
Band5	0.0125	85.72	65.29	0.0050	31.29	23.10	0.0045	32.81	9.16	**0.0034**	**21.34**	**−1.46**
Band6	0.0086	37.18	29.33	0.0052	17.73	13.78	**0.0042**	**16.80**	**−0.30**	0.0046	18.29	6.37
Band7	0.0064	33.90	23.63	**0.0041**	**18.00**	**4.71**	0.0042	23.65	9.85	0.0046	24.95	−1.09
Band8	0.0052	33.15	21.28	0.0037	18.76	6.07	**0.0035**	**18.44**	**−0.23**	0.045	30.13	−2.80
Band9	0.0050	34.43	20.49	0.0036	20.19	3.95	**0.0034**	**19.88**	**−0.15**	0.0045	32.99	−3.61
Band10	0.0048	32.26	18.44	0.0036	19.77	2.38	**0.0034**	**19.71**	**1.91**	0.0045	33.52	−5.02
Band11	0.0054	36.22	31.36	**0.0030**	**16.18**	**8.07**	0.0044	20.90	7.20	0.0047	32.94	−1.63
Band12	0.0048	88.38	66.65	**0.0017**	**36.40**	**22.80**	0.0026	33.16	15.77	0.0033	76.70	8.53
Band16	0.0041	67.89	49.21	**0.0012**	**21.36**	**5.51**	0.0030	37.88	23.63	0.0033	74.28	−1.50
Band17	0.0035	95.00	57.93	**0.0009**	**29.11**	**−16.92**	0.0016	33.92	−3.68	0.0035	145.43	−36.98
Band18	0.0034	110.29	65.18	0.0013	55.14	−50.78	**0.0014**	**34.86**	**−0.94**	0.0036	182.99	−59.68

overall application effectiveness is reduced [37], with RMSE ranging from 0.0026 to 0.0047 Sr^{-1} and MAPE ranging from 18.29% to 182.99%.

In bands 7–11, both C2RCC and 6S algorithms show the best correction accuracies, with MAPE around 20% and RMSE as low as 0.003 Sr^{-1}. In bands 12 and 16–18, the errors of the four algorithms are significantly higher than in the previous bands, but C2RCC exhibits relatively stable performance, with MAPE of 30%–40%. For longer wavelength bands, the remotely sensed reflectance is relatively poor. This may be explained by the strong absorption of colored dissolved organic matter, debris, and phytoplankton pigments in the violet band, coupled with the strong absorption of pure water in the infrared band. In this case, the contribution of water to the overall value is lower than that of the atmosphere, amplifying errors during correction [38]. The FLAASH algorithm yields corrected values higher than the measured reflectance in all Sentinel-3 bands. The correction results for C2RCC and 6S are also higher than the measured values, consistent with the results in Fig. 3. The ACOLITE algorithm produces correction results that are higher than the measured values in the violet band and lower in the near-infrared band, with the remaining bands having a BIAS of approximately 0. Therefore, the overall BIAS of ACOLITE shows the lowest absolute values [see Fig. 3(d)].

Based on the comprehensive analysis presented above, C2RCC yielded the best results among the tested algorithms, with RMSE consistently lower than 0.0051 Sr^{-1}, MAPE lower than 40% for all bands except bands 1–3, and an absolute BIAS lower than 23.63%.

B. Evaluation of the Adaptability of the TSM Inversion Algorithm

Herein, an empirical method was employed for estimating the TSM in the Nanyi Lake. Seventy percent of the data in the sample were randomly selected, and linear regression analysis of the measured TSM and the combination of various satellite bands was performed to construct the TSM inversion model.

TABLE IV
CORRELATIONS BETWEEN SENTINEL-3 OLCI BAND COMBINATIONS AND TSM

Inversion Factor	Optimal Band Combination	Correlation Coefficient
$\frac{B_m}{B_n}$	B12/B11	0.8130
$\frac{B_m - B_n}{B_m + B_n}$	(B11 − B16)/(B11 + B16)	0.8187
$\frac{B_m + B_n}{B_j}$	(B9 + B18)/B10	**0.8221**
$\frac{B_m - B_n}{B_j}$	(B18 − B10)/B9	0.8200
$\frac{B_m}{B_n - B_j}$	B9/(B10 − B18)	0.8218

Considering the high absorption and low reflection of water and building upon the selected atmospheric correction algorithm, a band combination model using the ratio method for inversion factors was employed. The ratio method can partially eliminate the effect of the atmosphere and reduce interference from changes in water surface roughness in space and time [39].

By calculating the CV, TSM data for 80 in situ points that met the conditions were screened. In the inversion of TSM in the Nanyi Lake, the band ratio and the three-band combination were utilized, and Pearson correlation analysis was then performed with the TSM values measured at the sampling points. The results of the correlation analysis for the selected band combinations are given in Table IV.

The 80 data points were randomly divided into training and testing sets in a 7:3 ratio. Using the training set, the specific expression for the inversion algorithm was determined using the inversion factors with high correlation coefficients, as given in Table V. Subsequently, the accuracy of the obtained algorithm was validated using the testing set. Finally, the results of TSM inversion at satellite points matching the measured concentration were compared to further validate the applicability of the algorithm. The specific results are given in Table V.

The results of the accuracy assessment show that the (B9 + B18)/B10 combination shows the best performance: R^2 of 0.76,

TABLE V
OPTIMAL INVERSION ALGORITHMS CONSTRUCTED ON THE BASIS OF TRAINING AND TEST SETS AND THEIR PERFORMANCE

Modeling Data (70%)		Validation Data (30%)		
Optimal Band Combination	Inversion Model	R^2	RMSE	MAPE (%)
$\frac{B_{12}}{B_{11}}$	$y = 202.76x - 54.25$	0.74	4.84	30.88
$\frac{B_{11}-B_{16}}{B_{11}+B_{16}}$	$y = -182.59x - 97.38$	0.73	5.01	31.93
$\frac{B_9+B_{18}}{B_{10}}$	$y = 254.55x - 262.37$	0.76	4.69	28.46
$\frac{B_{18}-B_{10}}{B_9}$	$y = -245.43x - 237.6$	0.76	4.73	28.74
$\frac{B_9}{B_{10}-B_{18}}$	$y = 191.95x - 196.85$	0.76	4.70	28.51

RMSE of 5.01 mg/L, and MAPE of 28.46% on the test set. Therefore, $y = 254.55x - 262.37$ was selected as the inversion algorithm for TSM in the Nanyi Lake.

IV. ANALYSIS OF TEMPORAL AND SPATIAL TSM VARIATIONS IN THE NANYI LAKE

Herein, the C2RCC algorithm was selected as the atmospheric correction algorithm for Sentinel-3 OLCI images. The selected inversion algorithm for the Nanyi Lake was applied to the images to obtain the monthly TSM concentration in the Nanyi Lake from 2018 to 2023. Because of the frequent occurrence of cloudy and rainy weather around the Nanyi Lake from June to September, in some cases, the entire month's images were invalid. In such cases, images from the three days before and after the month were selected as substitutes. If no valid images are available, the month is displayed as blank. The monthly distribution results for the Nanyi Lake are shown in Fig. 4.

The analysis of spatial and temporal changes in TSM is an effective means of monitoring the eutrophic status of the lake, enabling special management for the monitoring of whether the TSM is high in a specific area for a long time or whether TSM in the area considerably changes. To better discover the spatial variations in the TSM in the Nanyi Lake, the CV was calculated to quantify the degree of TSM variation, as shown in Fig. 5.

According to Fig. 5, TSM in most areas significantly changes from 2018 to 2023, particularly in the shoreline areas affected by human activities and regions where rivers converge [23]. The CV reaches approximately 2 in these areas, indicating a significant variation in TSM over the six years. In the central area of the lake, TSM variation is relatively small, resulting in a lower CV. In the southwestern region near the shoreline, where the concentration is more prone to changes, the CV reaches 1.4. Timely monitoring of TSM in these areas can allow to effectively manage suspended particulate matter concentrations in Nanyi Lake and protect the ecological environment.

To better understand the interannual TSM variation trends in the Nanyi Lake from 2018 to 2023, TSM values were averaged for the corresponding years, and the mean, maximum, and minimum values for the lake are plotted in Fig. 6.

Fig. 6 shows that the annual average TSM in the Nanyi Lake considerably varies, gradually decreasing from 2018 to 2020 and reaching a minimum in 2020. This significant TSM decline was attributed to the watershed water pollution control measures taken by the counties around the Nanyi Lake. According to the Xuancheng City Ecological Environment Bureau, the monitoring of the water quality for many months in 2019 showed that water in the lake did not meet the annual water quality III target requirements [40]. On July 30, 2019, the Municipal Bureau of Ecology and Environment commissioned a professional organization to prepare the "Nanyi Lake Water Pollution Comprehensive Treatment Implementation Plan." Therefore, to improve the quality of the water in the Nanyi Lake basin, the counties around it have actively performed special treatment actions. With the normalization of the treatment activities, the TSM in the Nanyi Lake tends to fluctuate and stabilize during 2021–2023. Owing to the implementation of the treatment activities, the TSM in the Nanyi Lake significantly improved in 2020 and is expected to stabilize after fluctuating in 2021–2023.

To more accurately analyze the temporal variation in the TSM in the Nanyi Lake, the monthly average concentration was calculated, as shown in Fig. 7.

According to Fig. 7 the data for June 2018 and 2019 is missing; at the same time, TSM consistently increases from May to July 2020–2023. Therefore, the average TSM values for May and July were calculated as the corrected values for the missing data in June for these two years. Because of the relatively small impact of other missing images on the overall trend, no other corrections were made. Considering seasonal variations, TSM in the Nanyi Lake gradually increases in spring and decreases in fall. This tendency was attributed to the temperature increase, increase in sunlight intensity, and the proliferation of phytoplankton and algae in spring, leading to an increase in TSM [41]. In contrast, with the onset of lower temperatures in autumn and a decrease in sunlight intensity, the concentration of organic suspended matter decreases. Overall, the TSM is relatively low in winter and spring and generally high in summer and fall. The monthly change in TSM in the Nanyi Lake shows a general trend of an increase followed by a decrease.

According to the satellite imagery combined with on-site observations, there are large areas of aquaculture and reclaimed land around the Nanyi Lake. Through visual interpretation, the aquaculture and reclaimed areas on the northwest, northeast, and southeast sides of the Nanyi Lake were extracted, consistent with the extraction range reported by Wang et al. [22], as shown in Fig. 8.

The TSM distribution map intuitively illustrates the TSM conditions in different areas of the Nanyi Lake, allowing for a better comparison of the differences in the TSM distribution between months.

According to Fig. 4, TSM in the three aquaculture reclamation areas to the northwest, northeast, and southeast of Nanyi Lake remains at relatively high levels for a long time, whereas TSM in the lake area fluctuates to varying degrees over time. According to statistics, in 2019, within a range of 1000 m along the coast of the Nanyi Lake and the main upstream rivers, there were 276 aquaculture farms and over 10 000 acres of aquaculture nets. These aquaculture and reclaimed areas lack corresponding pollution control measures, leading to a direct or indirect influx of pollutants into the Nanyi Lake [42]. Therefore, during 2018–2019, the overall TSM in the Nanyi Lake remains high,

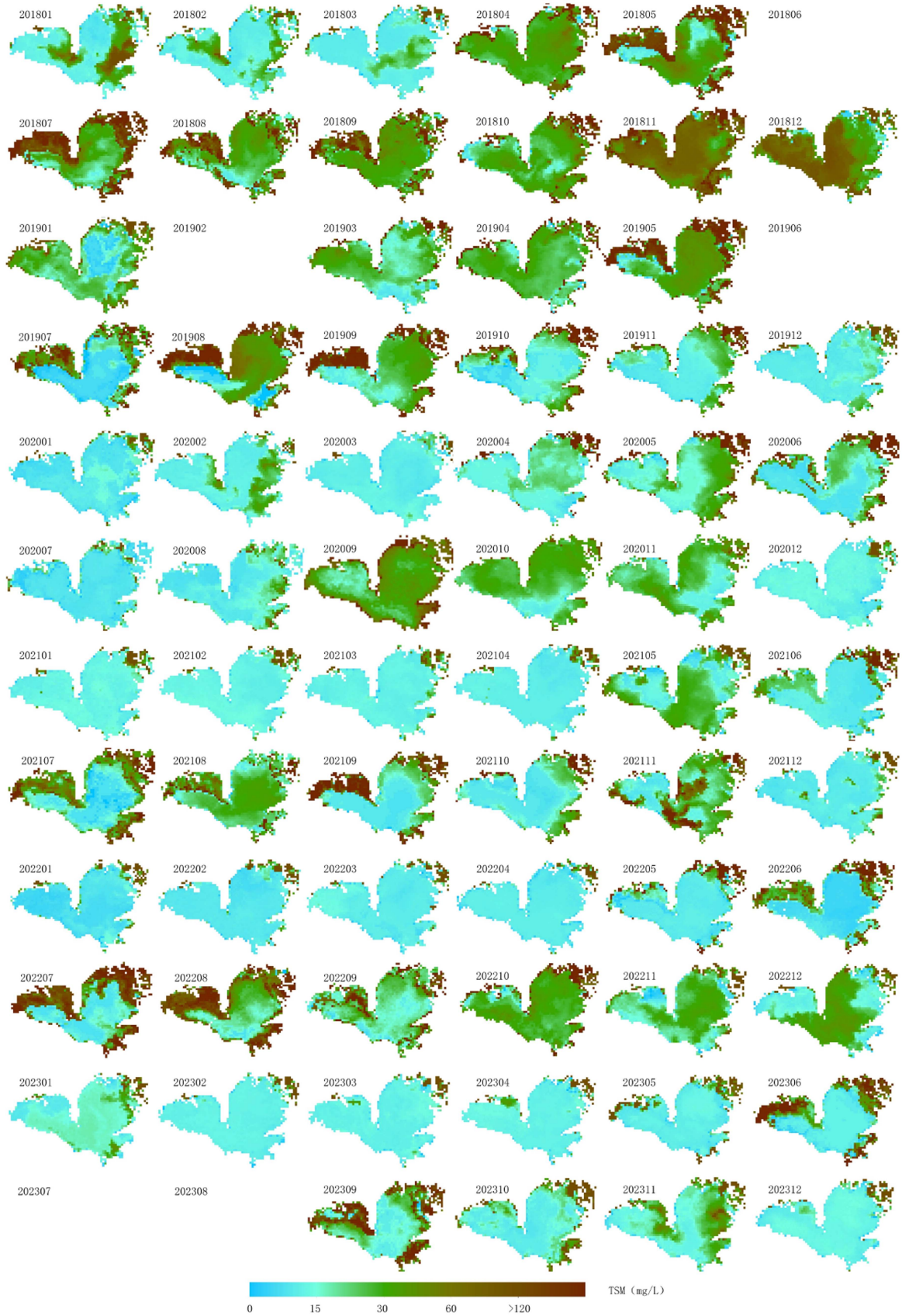

Fig. 4. Monthly TSM Distribution in the Nanyi Lake, 2018–2023.

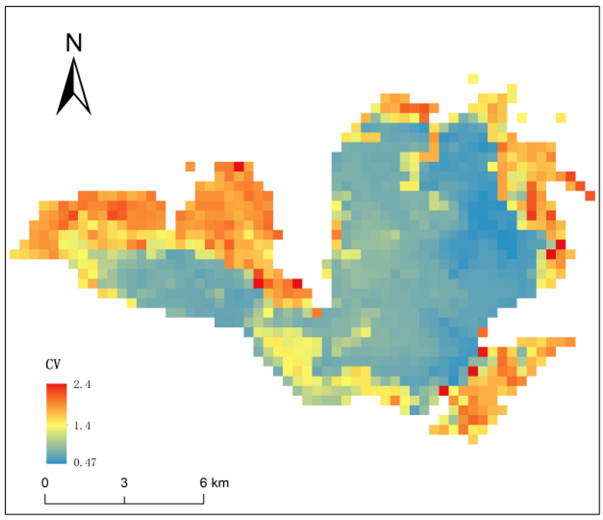

Fig. 5. CV distribution for TSM in the Nanyi Lake, 2018–2023.

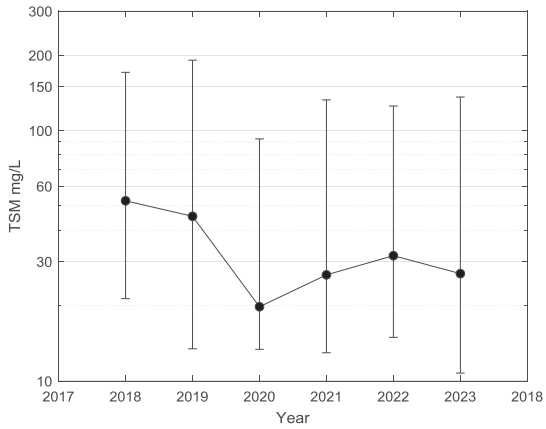

Fig. 6. Interannual statistics for TSM in the Nanyi Lake.

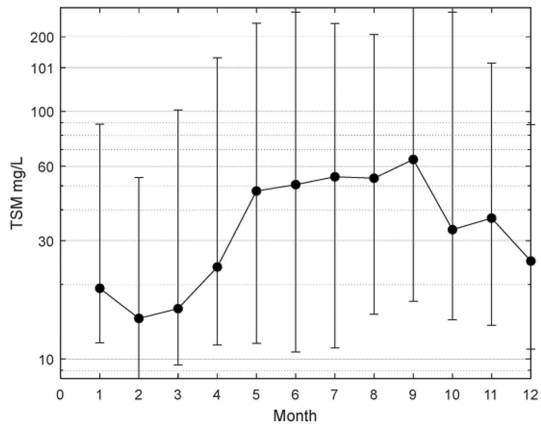

Fig. 7. Intermonthly Statistics for the TSM in the Nanyi Lake, 2018–2023.

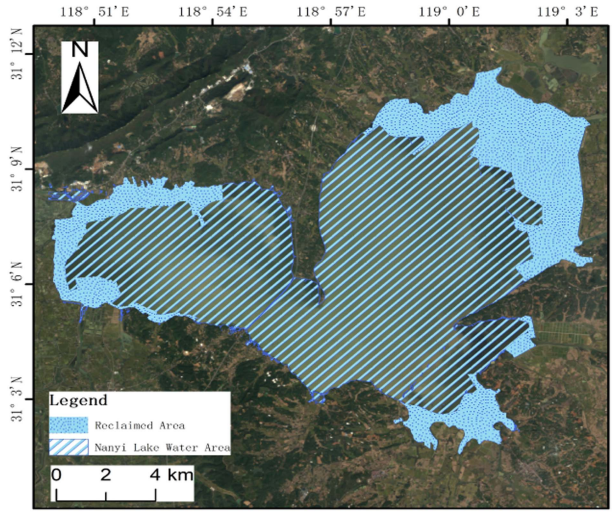

Fig. 8. Distribution of water area and reclaimed areas in the Nanyi Lake.

particularly in the lake area where TSM is generally greater than 30 mg/L. Furthermore, the areas with high TSM gradually expand.

In response to this tendency, the government and ecological environment management departments attached great importance to special remedial actions. In 2020, the TSM in the Nanyi Lake significantly decreased. The TSM values in July and August 2020 are significantly lower than those in other years. Investigations revealed that in 2020, the plum rain period lasted for 51 days, which was twice the historical average (25 days), and the rainfall was 935 mm, the second-highest since 1961 [43]. Owing to a significant increase in rainfall during the plum rain period, the increase in the Nanyi Lake's water storage volume led to a significant reduction in TSM.

During 2021–2023, TSM shows a similar pattern. During the period from January to May, the TSM is low in a relatively large part of the total area, while the high-TSM area gradually expands. From June to November, there is an area with TSM exceeding 120 mg/L, showing a trend of increasing followed by decreasing. By December, the TSM is generally lower. Therefore, TSM significantly varies in the Nanyi Lake, as regulated by various factors, including human activities, precipitation, temperature, and illumination.

V. Conclusion

Herein, Sentinel-3 OLCI satellite data was combined with remotely sensed reflectance and TSM data measured via navigational water experiments to assess the applicability of atmospheric correction and TSM inversion algorithms in the Nanyi Lake region as well as analyze the temporal and spatial variations in TSM from 2018 to 2023. The main research findings are as follows.

1) For the Sentinel-3 OLCI data, among the four tested atmospheric correction methods (FLAASH, 6S, ACOLITE, and C2RCC), the C2RCC algorithm showed overall stability and the highest accuracy (RMSE: 0.0014–0.0051 Sr^{-1}; MAPE: 18.44%–68.47%; BIAS: from −3.68% to 23.63%). The remaining three algorithms rank by accuracy in descending order as follows: ACOLITE, 6S, and FLAASH.
2) The three-band ratio combination (B9 + B18)/B10 exhibited the highest correlation with the in situ TSM. Thus,

this metric was used as the inversion factor to construct the inversion model: $y = 254.55x - 262.37$. The TSM inversion model constructed using this inversion factor showed good accuracy for the inversion of TSM concentration in the Nanyi Lake, with R^2 reaching 0.76, RMSE of 5.01 mg/L, and MAPE of 28.46%.

3) The temporal and spatial variations in the TSM in the Nanyi Lake exhibited significant regularities. In terms of temporal changes, the annual average TSM in the Nanyi Lake was 52.42, 45.45, and 19.78 mg/L in 2018–2020, respectively, showing a significant decreasing trend. In 2021–2023, the TSM tended to fluctuate and stabilize, with an annual average of approximately 28 mg/L. The seasonal TSM values, which are affected by factors such as human activities, precipitation, and illumination, follow the order of summer > autumn > spring > winter. Considering monthly variations in TSM in the Nanyi Lake, TSM initially increases followed by a decrease, with higher concentrations observed in July, August, and September. In terms of spatial variations, higher TSM values are observed in the northwest, northeast, and southeast reclamation areas and their surrounding lake areas, whereas the central lake area exhibited lower TSM values. Regions affected by river inflow and human activities show significant fluctuations in TSM from 2018 to 2023.

Although we selected an empirical model with high accuracy for Nanyi Lake, its strong regional dependence is notable. Future research endeavors could enhance the model's applicability by conducting in-depth analysis of the spectral characteristics of measured water reflectance, coupled with the integration of physical mechanisms.

ACKNOWLEDGMENT

The authors would like to acknowledge the space agencies around the globe for providing remote sensing data/information used in this article.

REFERENCES

[1] H. Li, L. Fan, L. Wang, J. Li, and L. Cui, "Remote sensing monitoring of suspended solids concentration in the three gorges reservoir area based on multi-source satellite data," *Resour. Environ. Yangtze Basin*, vol. 32, no. 3, pp. 611–625, 2023.

[2] Y. Du et al., "Using remote sensing to understand the total suspended matter dynamics in lakes across Inner Mongolia," *IEEE J. Sel. Topics Appl. Earth Observ. Remote Sens.*, vol. 14, pp. 7478–7488, Jul. 2021, doi: 10.1109/JSTARS.2021.3097083.

[3] K. E. Havens, "Submerged aquatic vegetation correlations with depth and light attenuating materials in a shallow subtropical lake," *Hydrobiologia*, vol. 493, pp. 173–186, 2003.

[4] X. Fang, Z. Wen, J. Chen, S. Wu, Y. Huang, and M. Ma, "Remote sensing estimation of suspended sediment concentration based on random forest regression model," *Remote Sens. Bull.*, vol. 23, no. 04, pp. 756–772, 2019.

[5] M. K. Stroud, G. H. Allen, M. Simard, D. Jensen, B. Gorr, and D. Selva, "Optimizing satellite mission requirements to measure total suspended solids in rivers," *IEEE Trans. Geosci. Remote Sens.*, vol. 62, pp. 1–9, Nov. 2023, Art. no. 4200409.

[6] J. Li, Y. Hao, Z. Zhang, Z. Li, R. Yu, and Y. Sun, "Analyzing the distribution and variation of suspended particulate matter (SPM) in the yellow river estuary (YRE) using landsat 8 OLI," *Regional Stud. Mar. Sci.*, vol. 48, 2021, Art. no. 102064.

[7] C. Jayaram, G. Patidar, D. Swain, V. M. Chowdary, and S. Bandyopadhyay, "Total suspended matter distribution in the Hooghly river estuary and the Sundarbans: A remote sensing approach," *IEEE J. Sel. Topics Appl. Earth Observ. Remote Sens.*, vol. 14, pp. 9064–9070, Sep. 2021, doi: 10.1109/JSTARS.2021.3076104.

[8] W. Zhou, "Monitoring of water quality parameters for inland waters by multi-spectral remote sensing data," M.S. thesis, Inst. Remote Sens. Digital Earth, Chin. Acad. Sci., Beijing, China, 2004.

[9] H. Li, J. Xu, X. Kui, Z. Huang, and R. Ma, "A dataset of suspended particulate matter concentration in Hulun Lake from2002 to 2021," *China Sci. Data*, vol. 8, no. 04, pp. 278–289, 2023.

[10] A. El-Alem, K. Chokmani, I. Laurion, and S. E. El-Adlouni, "Comparative analysis of four models to estimate chlorophyll-a concentration in case-2 waters using MODerate resolution imaging spectroradiometer (MODIS) imagery," *Remote Sens.*, vol. 4, no. 8, pp. 2373–2400, 2012.

[11] G. Jiang et al., "Remote sensing retrieval for chlorophyll-a concentration in turbid case waters (I):Application on MERIS image," *J. Infrared Millimeter Waves*, vol. 32, no. 04, pp. 372–378, 2013.

[12] H. Duan, Z. Deng, F. Deng, and A. Xu, "Research on remote sensing inversion of suspended matter concentration in Daihai lake based on QAA model," *Environ. Eng.*, vol. 36, no. 11, pp. 147–151, 2018.

[13] P. Wirabumi, M. Kamal, and P. Wicaksono, "Determining effective water depth for total suspended solids (TSS) mapping using planet scope imagery," *Int. J. Remote Sens.*, vol. 42, no. 15, pp. 5784–5810, 2021.

[14] D. Jensen et al., "Improving the transferability of suspended solid estimation in wetland and deltaic waters with an empirical hyperspectral approach," *Remote Sens.*, vol. 11, no. 13, 2019, Art. no. 1629.

[15] L. S. Kupssinskü et al., "Prediction of chlorophyll-a and suspended solids through remote sensing and artificial neural networks," in *Proc. 13th Int. Conf. Sens. Technol.*, 2019, pp. 1–6.

[16] J. Chen et al., "Remote sensing estimation of chlorophyll-A in case-II waters of coastal areas: Three-band model versus genetic algorithm–artificial neural networks model," *IEEE J. Sel. Topics Appl. Earth Observ. Remote Sens.*, vol. 14, pp. 3640–3658, Mar. 2021, doi: 10.1109/JSTARS.2021.3066697.

[17] L. S. Kupssinskü et al., "A method for chlorophyll-a and suspended solids prediction through remote sensing and machine learning," *Sensors*, vol. 20, no. 7, 2020, Art. no. 2125.

[18] X. Xie and Y. Chen, "Retrieval of total suspended matter in the lower of Minjiang river based on PSO-RBF," *Remote Sens. Technol. Appl.*, vol. 33, no. 05, pp. 900–907, 2018.

[19] D. Chen, Y. Chen, X. Feng, and S. Wu, "Retrieving suspended matter concentration in rivers based on hyperparameter optimized CatBoost algorithm," *Geo-Inf. Sci.*, vol. 24, no. 04, pp. 780–791, 2022.

[20] L. Wang, X. Wang, X. Wang, Q. Meng, Y. Ma, and Y. Chen, "Retrieval of suspended particulate matter concentration from Sentinel-3OLCl image in the coastal waters of Qinhuangdao," *China Environ. Sci.*, vol. 42, no. 08, pp. 3867–3875, 2022.

[21] X. Xu, F. Gao, and X. Yang, and C. Hu, "Temporal and spatial variation monitoring of water quality from Nanyi lake based on remote sensing data inversion, China," *Recyclable Res. Circle ECO*, vol. 13, no. 04, pp. 31–34, 2020.

[22] X. Wang et al., "Impact of lake areas on sediment accumulation rates and transportfluxes in Nanyi lake during the period of 1985-2016," *J. Environ. Eng. Technol.*, vol. 11, no. 06, pp. 1121–1130, 2021.

[23] W. Wei and S. Wang, "Impact analysis of the dredging project in Nanyi lake based on the MIKE model," *Shanxi Water Resour.*, no. 10, pp. 172–175, 2023.

[24] G. Lantzanakis, Z. Mitraka, and N. Chrysoulakis, "Comparison of physically and image based atmospheric correction methods for Sentinel-2 satellite imagery," in *Perspectives On Atmospheric Sciences*. Cham, Switzerland: Springer, pp. 255–261, 2017.

[25] F. Xie et al., "Characteristics of phosphorus fractions in sediments and its influence on the water quality of Lake Nanyi," *China Environ. Sci.*, vol. 42, no. 11, pp. 5318–5327, 2022.

[26] M. Zhai, Z. Tao, X. Zhou, and R. Li, "Water multi-parameter sampling design method based on adaptive sample points fusion in weighted space," *Remote Sens.*, vol. 14, 2022, Art. no. 2780.

[27] J. Tang, G. Tian, X. Wang, X. Wang, and Q. Song, "The methods of water spectra measurement and analysis i :Above-water method," *Remote Sens. Bull.*, vol. 01, pp. 37–44, 2004.

[28] C. Gao, J. Xu, D. Wang, and Y. Wang, "Retrieval of concentration of total suspended matter from GF-1 satellite and field measured spectral data during flood period in Poyang Lake," *Remote Sens. Land Resour.*, vol. 31, no. 01, pp. 101–109, 2019.

[29] J. Liu et al., "Spatial variability of soil salt in different soil layers at different scales," *J. Basic Sci. Eng.*, vol. 26, no. 02, pp. 305–312, 2018.
[30] Z. Lu, "Research on atmospheric correction method for multi-sourcesatellite remote sensing of inland water," Ph.D. dissertation, Inst. Remote Sens., Digital Earth, Chin. Acad. Sci., Beijing, China, 2019.
[31] Y. Liu, J. Li, C. Xiao, F. Zhang, and S. Wang, "Inland water chlorophyll-a retrieval based on ZY-1 02D satellite hyperspectral observations," *Remote Sens. Bull.*, vol. 26, no. 01, pp. 168–178, 2022.
[32] W. Shi and M. Wang, "Detection of turbid waters and absorbing aerosols for the MODIS ocean color data processing," *Remote Sens. Environ.*, vol. 110, no. 2, pp. 149–161, 2007.
[33] P. R. Renosh, D. Doxaran, L. D. Keukelaere, and J. I. Gossn, "Evaluation of atmospheric correction algorithms for sentinel-2-MSI and sentinel-3-OLCI in highly turbid estuarine waters," *Remote Sens.*, vol. 12, no. 8, 2020, Art. no. 1285.
[34] M. Asim, A. Matsuoka, P. G. Ellingsen, C. Brekke, T. Eltoft, and K. Blix, "A new spectral harmonization algorithm for Landsat-8 and Sentinel-2 remote sensing reflectance products using machine learning: A case study for the Barents sea (European arctic)," *IEEE Trans. Geosci. Remote Sens.*, vol. 61, pp. 1–19, Dec. 2023, Art. no. 4200819.
[35] C. Brockmann, R. Doerffer, M. Peters, S. Kerstin, S. Embacher, and A. Ruescas, "Evolution of the C2RCC neural network for Sentinel 2 and 3 for the retrieval of ocean colour products in normal and extreme optically complex waters," *Living Planet Symp.*, vol. 740, 2016, Art. no. 54.
[36] S. Li et al., "Performances of atmospheric correction processors for sentinel-2 MSI imagery over typical lakes across China," *IEEE J. Sel. Topics Appl. Earth Observ. Remote Sens.*, vol. 16, pp. 2065–2078, Jan. 2023, doi: 10.1109/JSTARS.2023.3238713.
[37] Y. Luo et al., "Evaluation of applicability of Sentinel-2-Sl and Sentinel-3-0LCl water leaving reflectance products in Yellow River Estuary," *Sci. Technol. Atmospheric Effects Opt.*, vol. 18, no. 06, pp. 585–601, 2023.
[38] P. Qin, S. G. Simis, and G. H. Tilstone, "Radiometric validation of atmospheric correction for MERIS in the Baltic Sea based on continuous observations from ships and AERONET-OC," *Remote Sens. Environ.*, vol. 200, pp. 263–280, 2017.
[39] Q. Huang, Z. He, H. Liang, Z. Yang, and X. Zeng, "Inversion of chlorophyll-a concentration in Baihua lake in Guiyang city based on HJ-1A CCD data," *Yangtze River*, vol. 50, no. 03, pp. 66–72, 2019.
[40] Y. Li, "Causes of total phosphorus exceedance in Nanyi lake and suggestions on the management of meeting the standard," *Anhui Agricultural Sci. Bull.*, vol. 26, no. 04, pp. 137–138, 2020.
[41] X. Xu, "The study of remote sensing imagery waterquality parameter algorithms and spatial and temporal patterns variation of water quality in lake Liangzi," Ph.D. dissertation, Wuhan Univ., Wuhan, China 2017.
[42] Z. Wu, H. Wang, P. Tang, and F. Zhang, "Change trends of water quality of Nanyi lake in 2011-2020," *Anhui Chem. Ind.*, vol. 48, no. 04, pp. 72–87, 2022.
[43] X. Zhong, J. Li, and J. Shi, and J. Zhang, "Analysis of rainstorm and flood characteristics of Yangtze river basin(Anhui region)during the East Asian rain season," *Exp. Water Resour. Hydropower Inf.*, vol. 43, no. 04, pp. 21–26, 2022.

Yong Xie (Senior Member, IEEE) received the B.S. and M.S. degrees in physics from the Nanjing Normal University, Nanjing, China, in 2000 and 2004, respectively, and the Ph.D. degree in earth science and geoinformation system from George Mason University, Fairfax, VA, USA, in 2009.

He is currently a Professor with the School of Geographical Science, Nanjing University of Information Science and Technology, Nanjing, China. He has worked on the radiomimetic calibration and characterization of satellite remote sensor and science product validation with ground measurements.

Yanting Zhou is currently working toward the master's degree in geography with Nanjing University of Information Science and Technology, Nanjing, China.

Her research interests include water quality parameter retrieval.

Zui Tao was born in China in 1984. He received the B.S. degree from Henan University, Kaifeng, China, in 2005, the M.S. degree from Wuhan University, Wuhan, China, in 2008, and the Ph.D. degree from the Institute of Remote Sensing and Digital Earth, Chinese Academy of Sciences (CAS), Beijing, China, in 2012, all in cartography and geographic information system.

He is currently a Research Assistant with the Aerospace Information Research Institute, CAS. His research interests include validation of remote sensing product, ecological, and environmental remote sensing

Wen Shao received the B.S. and M.S. degrees in electronic information from the Nanjing University of Information Science and Technology, Nanjing, China, in 2017 and 2020, respectively, where he is currently working toward the Ph.D. degree in 3S integration and meteorological applications.

His research interests include satellite sensor on-orbit radiometric calibration.

Meng Yang is currently working toward the master's degree in geography with Nanjing University of Information Science and Technology, Nanjing, China.

Her research interests include remote sensing monitoring, aiming to obtain high-frequency and fine surface environmental information.